Scientia Iranica F (2023) 30(6), 2245–2259

Sharif University of Technology
Scientia Iranica
Transactions F: Nanotechnology
http://scientiairanica.sharif.edu

Entropy generation on Darcy-Forchheimer flow of copper-aluminium oxide/water hybrid nanofluid over a rotating disk: Semi-analytical and numerical approaches

G. Ramasekhar and P. Bala Anki Reddy*

Department of Mathematics, S.A.S., Vellore Institute of Technology (VIT), Vellore-632014, India.

Received 15 March 2022; received in revised form 16 August 2022; accepted 21 May 2023

KEYWORDS
Darcy-Forchheimer;
Electromagnetohydrodynamic;
Porous medium;
Heat generation;
Viscous dissipation;
Thermal radiation.

Abstract. The proficiency of hybrid nanoparticles in increasing heat transfer has impressed many researchers to analyze the working of those fluids further. The current work studies the impact of entropy generation on electromagnetohydrodynamic (EMHD) hybrid nanofluid (copper-aluminum oxide) flow over a rotating disk in the presence of the porous medium, Darcy-Forchheimer, heat generation, viscous dissipation, and thermal radiation. By applying the self-similarity variables, the partial differential equations are converted into ordinary differential equations. After that, the dimensionless equations are numerically solved using the Runge-Kutta (R-K) technique, and the comparison is made between the numerical technique (R-K method) and the Homotopy Perturbation Method (HPM), where HPM yields a more effective and dependable conclusion. To highlight their physical significance, unique characteristic graphs are shown for the profiles of velocity, temperature, entropy generation, and Bejan number, along with a suitable explanation. The hybrid nanofluid velocity decreases with larger values of the magnetic parameter, but the velocity profile increases with the higher electric field. The findings are novel and innovative, with several modern industrial applications, and the results are in excellent concurrence with the relevant literature. Applications of the current research are refrigeration, electronics, heat exchangers, and lubricants.

1. Introduction

The rotating disk is a well-known geometry for studying various fluids because of its simplicity, and it stands as a classical fluid dynamics problem. Theoretically and practically, rotating disk circulation is advantageous. It is due to its numerous uses in viscometers, biomechanics, material handling engineering, and air cleaning equipment that incorporate medical equipment, oceanography, and other areas. Turning flows of electrically demanded fluids are used in computer storage devices and various other technological applications. Processes for crystal development and viscometers, as an example. Disk-shaped elements are used in many engineering processes, and the heat transfer issue over a revolving disk has been investigated by Shevchuk [1]. Biofuel generation, gas and aquatic turbines, and generators are a few applications for rotating disks in the automotive and energy sectors.

Nanofluids have a lengthy history of attracting the

*. *Corresponding author.*
E-mail address: pbarmaths@gmail.com (P. Bala Anki Reddy)

doi: 10.24200/sci.2023.60134.6617

attention of researchers from numerous fields of modern technology. The term "nanofluid" was developed by Choi and Eastman [2]. Researchers have been investigating a huge variety of advantages communicated to the heat transfer properties of nanofluids under the effect of a permeable medium in various geometries and motion scenarios over the past years. When suspended ultrafine nanoparticles (less than 100 nm) are present, this creation consists of a technology that enhances the thermal efficiency and convective heat transfer of base fluids such as ethylene, hydrology, and petroleum. The phenomenal aspect of this result motivated popular scientists to investigate the circulation and heat transfer of different nanofluids across various surfaces under multiple conditions to satisfy today's demands [3–5]. Several researchers have worked on the nanofluid models; see the references [6–9]. The concept of nanofluid has been expanded such that two or more nanoparticles may be dispersed into the base fluid at the same time. This new concept was given the term "hybrid nanofluid." Because of the enormous shift that this technology has brought about in the way that thermal and cooling systems are developed, hybrid nanofluids are being used to signal that there will likely be an improvement in the thermal performance of working fluids. It has been shown that increasing the number of different kinds of nanostructures in a fluid leads to an improvement in the fluid's ability to transmit heat. Numerous applications make use of hybrid nanofluids, including solar water heating, domestic refrigerators, heat exchangers, and converters. One example of such an application is the braking fluid in a car [10–14].

A magnetic field may be used to regulate free convection, and the magnetohydrodynamic (MHD) model is one of the most frequently used methods. MHD applications in revolving disk flow problems in research and technological innovation include weather forecasting and atomic power plants. The flow and heat transfer caused by rotating disks find usage in medical tools, aircraft engineering, and food processing technologies. Several researchers have used MHD nanofluid in theoretical and experimental studies [15–19] to investigate the rotating disk flow problem. In space technology, thermal radiation significantly impacts flow and heat transmission. High temperature and radiation-based technical methods are unquestionably important, and their implications must not be neglected. The effects of radiation on convective MHD flow problems improve electrical power generation, solar power technologies, and other manufacturing fields. As a result of the effects it has on application domains where thermal radiation and MHD are concerned, numerous researchers have expressed an interest in studying it. Many researchers [20–22] have continued their studies in adjacent fields. However, the electromagnetohydrodynamic (EMHD) effect is essential in theoretical and experimental studies in various fields, including biological and medical research, cardiology, skin problems, tumor and cancer treatment, radiofrequency ablation (RFA) [23], etc.

The significant response from the industrial fronts over heat transfer increases due to entropy formation prompted entropy generation. Entropy generation appears to be extraordinary in complex systems such as solid-state physics, magnetic refrigeration, and economic analysis of production systems, biochemistry, and biological systems [24]. It's important to keep in mind that the aim of the irreversibility process is intertwined with various thermal systems. Viscous dissipation, magnetic fields, Joule heating, heat and mass transport, and other techniques are all described using the idea of irreversibility. Many researchers employed the most efficient and reliable second rule of thermodynamics to enhance such irreversibility procedures. Several researchers have investigated entropy generation using a variety of models. Thermodynamics helps us understand how the brain works because it is a complicated system that undergoes energy and energy exchange. The creation of brain entropy can be very beneficial in both neurological and psychiatric studies of the brain and its diseases. Many scholars have attempted to invite solutions for fluid flow problems in the name of entropy minimization [25]. The total entropy generation may be affected by introducing nanoparticles to the working fluid. By employing nanofluids in the system, the temperature of the system can be reduced, and ultimately, the heat passing on involvement to the total entropy optimizing rate may be reduced. At the same time, the nano fragments increase the viscosity of the working fluid; thereby, the pressure drop in the operation increases. In the previous literature, many researchers calculated the entropy investigation, in turn, to obtain an optimal scenario for various thermal systems [26–29].

Over the last few decades, the significance of porous media has been recognized in a variety of industries. The porous medium enhances the contact area between liquid and solid surfaces and improves nanoparticle distribution, resulting in higher effective heat conductivity. Jakeer et al. [30] studied the influence of the permeable sheet with the Cattaneo-Christov heat flux model. As a consequence, typical thermal system efficiency is improved [31]. For flows with low porosity and low velocity, the well-known Darcy's law is enough. Darcy's law holds for low-flow rates across porous space (Re less than 1). For example, Darcy's law is useful for describing typical flows in porous areas; however, it is insufficient for flow rates. As a result, Forchheimer added a non-linear relationship between filtration velocity and pressure gradient to Darcy's equation. Darcy-Forchheimer relations were

used to study the disk flow of different fluids in a porous region [32]. The Forchheimer relation explains higher flow rates. Muskat and Wyckoff [33] also proclaimed it a "Forchheimer word" valid for a large Reynolds number. The attempts [34–37] show recent progress in this direction. Jakeer and Reddy [38] examined the Darcy-Forchheimer over a sheet.

To the best of the author's knowledge, there is no study on EMHD flow and heat transfer of hybrid nanofluid across a rotating disk with the effects of linear thermal radiation, porous, slip conditions, and viscous dissipation that has been done and taken into account. The governing Ordinary Differential Equations (ODEs) are transformed into partial differential equations through a similarity transformation and then solved using the Runge-Kutta (R-K) 4th order with the shooting technique. For comparison purposes, we used the Homotopy Perturbation Method (HPM) method. Al_2O_3-Cu/H_2O is considered. Copper (Cu) nanoparticles have smaller specific heat and a greater thermal conductivity, while Al_2O_3 solid particles have a larger specific heat and less thermal conductivity. The current study results are in excellent accord with the relevant literature. Many modern industries use them as heat exchangers and lubricants. The fundamental graphs and tables are represented in this current work.

2. Mathematical formulation

We consider a steady Darcy-Forchheimer flow of hybrid nanofluid over a stretching/shrinking rotating disk with viscous dissipation, porous medium, heat generation, and thermal radiation. In this study, (H_2O) is considered as base fluid, and (Al_2O_3-Cu) is taken as a hybrid nanoparticle. Darcy-Forchheimer and porous medium are explained in the momentum equations, represented in Eqs. (2) and (3). Heat generation, EMHD, and thermal radiation are explained as energy equations. The mathematical form of the energy equation is represented in Eq. (5). At $z = 0$, the disk rotates at a constant angular velocity Ω. The velocity components (u, v, w) are in increasing (r, ϕ, z) directions, respectively, as shown in Figure 1.

The governing boundary layer equations are [39]:

$$\frac{\partial u}{\partial r} + \frac{u}{r} + \frac{\partial w}{\partial z} = 0, \tag{1}$$

$$u\frac{\partial u}{\partial r} - \frac{v^2}{r} + w\frac{\partial u}{\partial z} = -\frac{1}{\rho_{hnf}}\frac{\partial p}{\partial r} + \frac{\mu_{hnf}}{\rho_{hnf}}\left(\frac{\partial^2 u}{\partial r^2} + \frac{1}{r}\frac{\partial u}{\partial r} - \frac{u}{r^2} + \frac{\partial^2 u}{\partial z^2}\right) - \frac{\mu_{hnf}}{\rho_{hnf}}\frac{u}{K^*} - F^* u^2 + \frac{\sigma_{hnf}}{\rho_{hnf}}\left(EB - B^2 u\right), \tag{2}$$

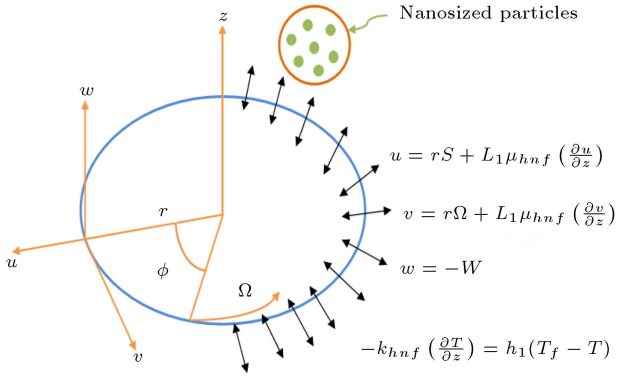

Figure 1. Geometrical configuration and coordinate system of the model.

$$u\frac{\partial v}{\partial r} + \frac{uv}{r} + w\frac{\partial v}{\partial z} = -\frac{1}{\rho_{hnf}}\frac{\partial p}{\partial \Theta} + \frac{\mu_{hnf}}{\rho_{hnf}}\left(\frac{\partial^2 v}{\partial r^2} + \frac{1}{r}\frac{\partial v}{\partial r} - \frac{v}{r^2} + \frac{\partial^2 v}{\partial z^2}\right) - \frac{\mu_{hnf}}{\rho_{hnf}}\frac{v}{K^*} - F^* v^2 + \frac{\sigma_{hnf}}{\rho_{hnf}}\left(EB - B^2 v\right), \tag{3}$$

$$u\frac{\partial w}{\partial r} + w\frac{\partial w}{\partial z} = -\frac{1}{\rho_{hnf}}\frac{\partial p}{\partial z} + \frac{\mu_{hnf}}{\rho_{hnf}}\left(\frac{\partial^2 w}{\partial r^2} + \frac{1}{r}\frac{\partial w}{\partial r} + \frac{\partial^2 w}{\partial z^2}\right), \tag{4}$$

$$u\frac{\partial T}{\partial r} + w\frac{\partial T}{\partial z} = \frac{k_{hnf}}{(\rho c_p)_{hnf}}\left(\frac{\partial^2 T}{\partial r^2} + \frac{1}{r}\frac{\partial T}{\partial r} + \frac{\partial^2 T}{\partial z^2}\right) + \frac{16\sigma^* T_\infty^3}{3k^*(\rho c_p)_{hnf}}\left(\frac{\partial^2 T}{\partial r^2} + \frac{1}{r}\frac{\partial T}{\partial r} + \frac{\partial^2 T}{\partial z^2}\right) + \frac{Q_0}{(\rho c_p)_{hnf}}(T - T_\infty) + 2\frac{\mu_{hnf}}{(\rho c_p)_{hnf}}\left[\left(\frac{\partial u}{\partial r}\right)^2 + \frac{u^2}{r^2} + \left(\frac{\partial w}{\partial z}\right)^2\right] + \frac{\mu_{hnf}}{(\rho c_p)_{hnf}}\left[\left(\frac{\partial v}{\partial z}\right)^2 + \left(\frac{\partial w}{\partial r} + \frac{\partial u}{\partial z}\right)^2 + \left\{r\frac{\partial}{\partial r}\left(\frac{v}{r}\right)\right\}^2\right] + \frac{\sigma_{hnf}}{(\rho c_p)_{hnf}}(uB - E)^2. \tag{5}$$

With:

$$u = rS + L_1\mu_{hnf}\left(\frac{\partial u}{\partial z}\right), \quad v = r\Omega + L_1\mu_{hnf}\left(\frac{\partial v}{\partial z}\right),$$

$$w = -W,$$

$$-k_{hnf}\left(\frac{\partial T}{\partial z}\right)=h_f\left(T_f-T\right) \quad \text{at} \quad z=0, \quad u\to 0,$$

$$v\to 0, \quad T\to T_\infty, \quad \text{as} \quad z\to\infty. \tag{6}$$

Mathematical models of the thermophysical properties of hybrid nanofluid are as follows:

$$A_1=\frac{\mu_{hnf}}{\mu_f}, \qquad A_2=\frac{\rho_{hnf}}{\rho_f}, \qquad A_3=\frac{\sigma_{hnf}}{\sigma_f},$$

$$A_4=\frac{(\rho c_p)_{hnf}}{(\rho c_p)_f}, \qquad A_5=\frac{k_{hnf}}{k_f}. \tag{7}$$

Eq. (8) is shown in Box I. Suitable self-similarity variables are expressed as follows:

$$(u,v,w)=\left(r\Omega F'(\eta), r\Omega G(\eta), -\sqrt{2\Omega v_f}F(\eta)\right),$$

$$(p,T)=\left(p_\infty-\Omega\mu_f p(\eta), T_\infty+(T_f-T_\infty)\theta\right),$$

$$\eta=\sqrt{\frac{2\Omega}{v_f}}z. \tag{9}$$

Now substituting Eq. (9) into the Eqs. (2) to (6) gives:

$$\frac{A_1}{A_2}\left(2F'''-KF'\right)+2FF''-F'^2+G^2-FrF'^2 + \frac{A_3}{A_2}M\left(E_1-F'\right)=0. \tag{10}$$

$$\frac{A_1}{A_2}\left(2G''-KG\right)+2FG'-2F'G-FrG^2 + \frac{A_3}{A_2}M\left(E_1-G\right)=0. \tag{11}$$

$$\frac{1}{A_4}\left(A_5+\frac{4}{3}Rd\right)\theta''+Pr\left[F\theta'+\frac{A_1}{A_4}6\left(\frac{Ec}{Re}\right)F'^2 + \frac{A_1}{A_4}Ec\left(F''^2+G'^2\right)+\frac{Q\theta}{2A_4}\right] + \frac{A_3}{A_4}MEcPr(F'-E_1)^2=0. \tag{12}$$

Boundary conditions (6) are transformed as below:

$$F'=\gamma+\delta\Gamma F'', \quad G=1+\delta\Gamma G', \quad F=Y,$$

$$\left(A_5\right)\theta'=-Bi\left(1-\theta\right), \quad \text{at} \quad \eta=0,$$

$$F'\to 0, \quad G\to 0, \quad \theta\to 0, \quad \text{as} \quad \eta\to\infty, \tag{13}$$

where γ is the stretching/shrinking rotating disk. Here, $\gamma>0$ indicates stretching rotating disk, while $\gamma<0$ indicates shrinking rotating disk. and:

$$K=\frac{v_f}{\Omega K^*}, \qquad Re=r\left(\frac{r\Omega}{v_f}\right),$$

$$\delta=\frac{1}{(1-\phi_1)^{2.5}(1-\phi_2)^{2.5}}, \qquad Fr=\frac{C_d}{\sqrt{K^*}},$$

$$E_1=\frac{E}{B\Omega r}, \qquad Y=\frac{W}{\sqrt{2\Omega v_f}}, \qquad Pr=\frac{v_f}{\alpha_f},$$

$$Rd=\frac{4\sigma^*T_\infty^3}{k^*k_f}, \qquad Ec=\frac{r^2\Omega^2}{(Cp)_f(T_f-T_\infty)},$$

$$\gamma=\frac{S}{\Omega}, \qquad Q=\frac{Q_0}{\Omega(\rho C_p)_f}, \qquad \Gamma=L_1\mu_f\sqrt{\frac{2\Omega}{v_f}},$$

$$Bi=\frac{h_f}{k_f}\sqrt{\frac{v_f}{2\Omega}}, \qquad M=\frac{\sigma_f B_0^2}{\Omega\rho_f}. \tag{14}$$

The skin friction coefficient and Nusselt number in the dimensional form are:

$$C_f=\frac{\sqrt{\tau_r^2+\tau_\varphi^2}}{\rho_f(r\Omega)^2}, \tag{15}$$

$$Nu_r=-\left(k_{hnf}+\frac{16\sigma^*T_\infty^3}{3k_fk^*}\right)-\frac{r\left(\frac{\partial T}{\partial z}\right)_{z=0}}{(T_f-T_\infty)}, \tag{16}$$

where:

$$\tau_r=\mu_{hnf}\left(\frac{\partial u}{\partial z}+\frac{\partial w}{\partial r}\right)_{z=0}=\mu_{hnf}(r\Omega)\sqrt{\frac{2\Omega}{v_f}}F''(0), \tag{17}$$

$$\tau_\varphi=\mu_{hnf}\left(\frac{\partial v}{\partial z}+\frac{\partial w}{\partial r}\right)_{z=0}=\mu_{hnf}(r\Omega)\sqrt{\frac{2\Omega}{v_f}}G'(0). \tag{18}$$

$$\left.\begin{array}{l} A_1=\frac{1}{(1-\phi_1)^{2.5}(1-\phi_2)^{2.5}},\\ A_2=\left\{(1-\phi_2)\left[(1-\phi_1)+\phi_1\left(\frac{\rho_{s_1}}{\rho_f}\right)\right]+\phi_2\frac{\rho_{s_2}}{\rho_f}\right\},\\ A_3=\frac{\sigma_{s_2}+2\sigma_{nf}-2\phi_2(\sigma_{nf}-\sigma_{s_2})}{\sigma_{s_2}+2\sigma_{nf}+\phi_2(\sigma_{nf}-\sigma_{s_2})}\times\frac{\sigma_{s_1}+2\sigma_f-2\phi_1(\sigma_f-\sigma_{s_1})}{\sigma_{s_1}+2\sigma_f+\phi_1(\sigma_f-\sigma_{s_1})},\\ A_4=(1-\phi_2)\left[(1-\phi_1)+\phi_1\left(\frac{(\rho c_p)_{s_1}}{(\rho c_p)_f}\right)\right]+\phi_2\frac{(\rho c_p)_{s_2}}{(\rho c_p)_f},\\ A_5=\frac{k_{s_1}+2k_{bf}-2\phi_2(k_{bf}-k_{s_2})}{k_{s_2}+2k_{bf}+\phi_2(k_{bf}-k_{s_2})}\times\frac{k_{s_1}+2k_f-2\phi_1(k_f-k_{s_1})}{k_{s_1}+2k_f+\phi_1(k_f-k_{s_1})}. \end{array}\right\}. \tag{8}$$

Box I

The non-dimensional skin friction coefficient and Nusselt number are expressed as follows:

$$(Re_r)^{1/2}C_f = \sqrt{2}A_1\sqrt{[F''(0)]^2 + [G'(0)]^2}, \quad (19)$$

$$(Re_r)^{-1/2}Nu_r = -\sqrt{2}\left(\frac{k_{hnf}}{k_f} + \frac{4}{3}Rd\right)\theta'(0), \quad (20)$$

where Re_r is the local Reynolds number $Re_r = \frac{r(r\Omega)}{\upsilon_f}$.

2.1. Entropy generation

The entropy generation of the hybrid nanofluid in the existence of thermal radiation, Joule heating, porosity, and viscous dissipation is given by Ramasekhar and Reddy [40]:

$$\begin{aligned} S'''_{gen} = {} & \frac{k_f}{T_\infty^2}\left[\frac{k_{hnf}}{k_f} + \frac{16\sigma^* T_\infty^3}{3k^* k_f}\right]\left(\frac{\partial T}{\partial z}\right)^2 \\ & + \frac{\mu_{hnf}}{T_w}\left\{2\left[\left(\frac{\partial u}{\partial r}\right)^2 + \frac{1}{r^2}u^2 + \left(\frac{\partial w}{\partial z}\right)\right]\right. \\ & \left. + \left(\frac{\partial v}{\partial z}\right)^2 + \left(\frac{\partial u}{\partial z}\right)^2 + \left[r\frac{\partial}{\partial r}\left(\frac{v}{r}\right)\right]^2\right\} \\ & + \frac{\mu_{hnf}}{K^* T_w}\left(u^2 + v^2\right) + \frac{\sigma_{hnf}}{T_w}\left(uB^2 - EB\right)^2. \end{aligned} \quad (21)$$

The entropy generation number N_G becomes:

$$\begin{aligned} N_G = \frac{S'''_{gen}}{2\left(k_f \Delta T\Omega/T_w \upsilon_f\right)} = {} & \alpha\left(A_5 + \frac{4}{3}Rd\right)(\theta')^2 \\ & + \frac{Br}{(1-\phi_1)^{2.5}(1-\phi_2)^{2.5}}\left[\frac{6}{Re}\{F'(\eta)\}^2\right. \\ & \left. + D^2\left(\{F''(\eta)\}^2 + \{G'(\eta)\}^2\right)\right] \\ & + \frac{BrK}{2(1-\phi_1)^{2.5}(1-\phi_2)^{2.5}}\left(F'^2 + G^2\right) \\ & + \frac{1}{2}MBr(F'-E)^2. \end{aligned} \quad (22)$$

The Bejan number obtained by Eq. (23) as shown in Box II.

3. Method of solution

3.1. Numerical scheme

The non-dimensional system of Eqs. (10)–(12), as well as the boundary conditions (13), were numerically solved by using the R-K 4th order along with the shooting technique. First, we converted the basic differential equations into a collection of first-order ODEs for this scheme.

$$F = m_1, \quad F' = m_2, \quad F'' = m_3, \quad G = m_4,$$
$$G' = m_5, \quad \theta = m_6, \quad \theta' = m_7. \quad (24)$$

Using Eq. (20), Eqs. (10)–(13) take the following form

$$\begin{aligned} F''' = {} & -\frac{1}{2\left(\frac{A_1}{A_2}\right)}\left[-\frac{A_1}{A_2}Km_2 + 2m_1m_2 - (m_2)^2\right. \\ & \left. + m_4^2 - Frm_2^2 + \frac{A_3}{A_2}M(E_1 - m_2)\right], \end{aligned} \quad (25)$$

$$\begin{aligned} G'' = {} & -\frac{1}{\left(\frac{A_1}{A_2}\right)}\left[-K\left(\frac{A_1}{A_2}\right)m_4 + 2m_1m_5 - 2m_2m_4\right. \\ & \left. - Fr(m_4)^2 + \frac{A_3}{A_2}M(E_1 - m_4)\right], \end{aligned} \quad (26)$$

$$\begin{aligned} \theta'' = {} & -\frac{Pr}{\left(A_4\left(A_5 + \frac{4}{3}Rd\right)\right)}\left[m_1m_7 + 6\left(\frac{A_1}{A_4}\right)\left(\frac{Ec}{Re}\right)(m_2)^2\right. \\ & + Ec\left(\frac{A_1}{A_4}\right)\left((m_3)^2 + (m_5)^2\right) + \frac{1}{2}A_4Qm_6 \\ & \left. + \frac{A_3}{A_4}MEc(m_2 - E_1)^2\right]. \end{aligned} \quad (27)$$

The boundary conditions for the corresponding boundary conditions are as follows:

$$\begin{aligned} & m_1(0) = Y, \quad m_2(0) = \gamma + \delta\Gamma m_3(0), \\ & m_4(0) = 1 + \delta\Gamma m_5(0), \\ & A_5\ m_7(0) = -Bi(1 - m_6(0)), \quad m_2(\infty) \to 0, \\ & m_4(\infty) \to 0, \quad m_6(\infty) \to 0. \end{aligned} \quad (28)$$

$$Be = \frac{\alpha\left(A_5 + \frac{4}{3}Rd\right)(\theta')^2}{\begin{array}{l}\alpha\left(A_5 + \frac{4}{3}Rd\right)(\theta')^2 + \frac{Br}{(1-\phi_1)^{2.5}(1-\phi_2)^{2.5}}\left[\frac{6}{Re}\{F'(\eta)\}^2 + D^2\left(\{F''(\eta)\}^2 + \{G'(\eta)\}^2\right)\right] \\ + \frac{BrK}{2(1-\phi_1)^{2.5}(1-\phi_2)^{2.5}}\left(F'^2 + G^2\right) + \frac{1}{2}MBr(F'-E)^2\end{array}}. \quad (23)$$

Box II

3.2. Analysis of HPM

A HPM can be developed as follows. By consider the following equations:

$$\vee(\lambda) - \ell(z) = 0, z \in \psi. \tag{29}$$

With the boundary conditions:

$$\dagger\left(\lambda, \frac{\partial\lambda}{\partial n}\right) = 0, z \in \partial\psi. \tag{30}$$

Here $\partial\psi$ is the boundary of the domain ψ, $\ell(z)$ is the analytic function. $\vee(\lambda)$ is the nonlinear differential operator and $\dagger$ is a boundary operator.

η is divided into two parts: linear L and nonlinear N:

$$L(\lambda) + N(\lambda) = \ell(z). \tag{31}$$

The structure of the HPM is delivered as follows:

$$G(\lambda, \eta) = (1-P)[L(\lambda) - L(\lambda_0)] + P[\vee(\lambda) - \ell(z)] = 0, \tag{32}$$

where:

$$\lambda(z, \eta): \psi \times [0,1] \to S_1. \tag{33}$$

In which $\eta \in [0,1]$ is an implementing parameter and λ_0 is the primary estimate of Eq. (29) capturing the boundary conditions.

The above solution may be expressed as a power series in η:

$$\lambda = \lambda_0 + \eta\lambda_0 + \eta^2\lambda_0 + ...$$

The exact approximation for the solution is $\eta = 1$.

$$\lambda = \lambda_0 + \lambda_1 + \lambda_2 + ...$$

3.3. Implementation of the method (HPM)

Employing Eqs. (10)–(13), the HPM pattern can be written as follows:

$$(1-P)\left(\frac{A_1}{A_2}(2)\right)F''' + P\left(\frac{A_1}{A_2}(2F''' - KF')\right) - P\left(F'^2\right) + P\left(G^2\right) - P\left(FrF'^2\right) + P\left(\frac{A_3}{A_2}M(E_1 - F')\right), \tag{34}$$

$$(1-P)\left(\frac{A_1}{A_2}(2)\right)G'' + P\left(\frac{A_1}{A_2}(2G'' - KG)\right) + P(2FG') - P(2F'G) - P\left(FrG^2\right) + P\left(\frac{A_3}{A_2}M(E_1 - G)\right), \tag{35}$$

$$(1-P)\left(\frac{1}{A_4}\left(A_5 + \frac{4}{3}Rd\right)\right)\theta'' + P\left(\left(\frac{1}{A_4}\left(A_5 + \frac{4}{3}Rd\right)\right)\right) + P\left(Pr\left[F\theta' + \frac{A_1}{A_4}6\left(\frac{Ec}{Re}\right)F'^2 + \frac{A_1}{A_4}Ec\left(F''^2 + G'^2\right) + \frac{Q\theta}{2A_4}\right]\right) + P\left(\frac{A_3}{A_4}MEcPr(F' - E_1)^2\right). \tag{36}$$

Boundary conditions are:

$$F'(0) = \gamma + \delta\Gamma F''(0), \qquad G(0) = 1 + \delta\Gamma G'(0),$$
$$F(0) = Y, \quad (A_5)\theta'(0) = -Bi(1 - \theta(0)) \quad \text{at} \quad \eta = 0,$$
$$F'(\infty) \to 0, \quad G(\infty) \to 0, \quad \theta(\infty) \to 0, \quad \text{as} \quad \eta \to \infty. \tag{37}$$

We consider F, G, θ, and N_G as follows:

$$F(x) = F_0(x) + \eta F_1(x) + \eta^2 F_2(x) + ..., \tag{38}$$

$$G(x) = G_0(x) + \eta G_1(x) + \eta^2 G_2(x) + ..., \tag{39}$$

$$\theta(x) = \theta_0(x) + \eta\theta_1(x) + \eta^2\theta_2(x) + ..., \tag{40}$$

$$N_G(x) = N_{G0}(x) + \eta N_{G1}(x) + \eta^2 N_{G2}(x) + ... \tag{41}$$

To make Eqs. (38)–(41) in the form of Eqs. (34)–(36), the coefficient of identical powers of η are compared, and then the obtaining linear equation system is solved to obtain:

Zeroth-order:

$$F_0 = \frac{A_1}{A_2}F'''(0) = 0, \tag{42}$$

$$G_0 = 2\frac{A_1}{A_2}G''(0) = 0, \tag{43}$$

$$\theta_0 = \frac{1}{A_3}\theta''(0) = 0, \tag{44}$$

$$N_{G0} = \frac{BrDF_2''^2}{A_1} = 0, \tag{45}$$

where zeroth-order conditions are:

$$F_0'(0) = \gamma + \delta\Gamma F_0''(0), \qquad G_0(0) = 1 + \delta\Gamma G_0'(0),$$
$$F_1(0) = Y, \qquad (A_5)\theta_0'(0) = -Bi(1 - \theta_0(0)). \tag{46}$$

First order:

$$F_1 = -FrF_0'^2 + 2F_0F_0'' + G_0^2 - F_0'^2 + \frac{A_1}{A_2}F_0''' - \frac{A_3}{A_2}MF_0' + \frac{A_3}{A_2}ME_1 - \frac{A_1}{A_2}KF_0' = 0, \quad (47)$$

$$G_1 = -KG_0 + 2F_0G_0' - 2F_0'G_0 - FrG_0^2 + 2\frac{A_1}{A_2}G_1'' - \frac{A_3}{A_2}MG_0' + \frac{A_3}{A_2}ME_1 = 0, \quad (48)$$

$$\theta_1 = \frac{A_5}{A_4}\theta_0'' + \frac{4}{3A_4}Rd\theta_0'' - 2E_1F_0' - \frac{1}{A_4}\theta_0'' + E_1^2 + MEcPrF_0'^2 + PrF_0\theta_0' + 6Pr\left(\frac{Ec}{Re}\right)\frac{A_1}{A_4}F_0'^2 + \frac{A_1}{A_4}PrEc\theta_0''^2 + \frac{A_1}{A_4}PrEcG_0'^2 = 0, \quad (49)$$

$$N_{G1} = \alpha\theta_0'^2A_5 + \frac{4}{3}\alpha\theta_0'^2Rd + \frac{6BrF_0'^2}{A_1Re} + \frac{BrDG_0'^2}{A_1} + \frac{Br^2KF_0'^2}{2A_1^2} + \frac{BrG_0^2}{A_1} + \frac{MBr}{2}F_0' - \frac{1}{2}MBr\left(F_0'^2 + G_0^2 + E_1\right) = 0, \quad (50)$$

where first-order conditions are:

$$F_1(0) = Y, \quad F_1'(0) = \gamma + \delta\ \Gamma F_1''(0), \quad F_1'(1) = 0,$$

$$G_1(0) = 1 + \delta\ \Gamma G_1'(0), \qquad G_1(1) = 0,$$

$$(A_5)\,(\theta_1'(0)) = -Bi\,(1 - \theta_1(0))\,, \qquad \theta_1(1) = 0. \quad (51)$$

Second order:

$$F_2 = \frac{2A_1\ F_2'''}{A_2} - 2\ Fr\ F_0'\ F_1' - \frac{A_3}{A_2}\ M\ F_1' + 2F_0F_1' + 2F_1F_0'' - 2F_0'F_1' + 2G_0G_1 + \frac{2A_1F'''}{A_2\beta} - \frac{A_1KF_1'}{A_2} = 0, \quad (52)$$

$$G_2 = 2F_1G_0' - 2F_0'G_1 - 2F_1'G_0 - KG_1 + 2F_0G_1' + 2\frac{A_1}{A_2}G_2'' - 2FrG_0G_1 - \frac{A_3}{A_2}MG_1' = 0, \quad (53)$$

$$\theta_2 = \frac{1}{A_4}\theta_2'' - 2E_1F_1' + PrF_1\theta_0' + PrF_1\theta_1' + \frac{4}{3A_4}Rd\theta_1'' + 2\frac{A_1}{A_4}PrEcF_0''F_1'' + 2\frac{A_1}{A_4}PrEcG_0'G_1' + 2MPrEcF_0'F_1' + 12Pr\frac{A_1}{A_4}\left(\frac{Ec}{Re}\right)F_0'F_1' + \frac{1}{2A_4}PrQ\theta_1 + \frac{1}{A_4}\theta_1' = 0, \quad (54)$$

$$N_{G2} = \frac{1}{2}\ M\ Br\ F_1' + \frac{Br\ D\ F_1^2}{A_1} + 2\alpha\ Rd\ \theta_0'\ \theta_1' + \frac{2\ Br\ G_0G_1}{A_1} + \frac{2Br\ D\ G_0'\ G_1'}{A_1} + \frac{Br^2\ K\ F_0'\ F_1'}{A_1^2} + \frac{2\ Br\ D\ F_0^2\ F_2^2}{A_1} + \frac{12\ Br\ F_0'F_1'}{A_1Re} = 0, \quad (55)$$

where second-order conditions are:

$$F_2(0) = Y, \quad F_2'(0) = \gamma + \delta\ \Gamma F_2''(0), \quad F_2'(1) = 0,$$

$$G_2(0) = 1 + \delta\ \Gamma G_2'(0), \qquad G_2(1) = 0,$$

$$(A_5)\,(\theta_2'(0)) = -Bi\,(1 - \theta_2(0))\,, \qquad \theta_2(1) = 0. \quad (56)$$

HPM solutions for F, G and θ at $K = 0.5$, $Fr = 0.1$, $M = 1.2$, $Rd = 0.1$, $Ec = 0.7$, $Re = 0.7$, $Q = 0.7$, $Pr = 6.20$, $Y = 0.5$, $E_1 = 0.5$, $\delta = 0.6$, $\Gamma = 0.5$, $\Omega = 0.9$, $Bi = 0.9$, $\eta = 0.2$, $\gamma = 0.5$, are given as follows by determining a series of functions:

$$\begin{aligned} F(\eta) = {} & 2.989422054\eta + 0.0002652519043\eta^9 \\ & - 0.00002824078984\eta^{10} - 0.000002515655145\eta^{11} \\ & + 1.141626929\eta^3 - 2.851429966\eta^2 \\ & + 0.03694421413\eta^6 - 0.008326747357\eta^7 \\ & + 0.0004496379456\eta^8 - 0.07724355910\eta^5 \\ & - 0.1235693645\eta^4 + 2.000000000, \end{aligned}$$

$$\begin{aligned} G(\eta) = {} & -5.526444844\eta + 3.304632524 \\ & + 0.4501105604\eta^4 - 1.244910195\eta^3 \\ & + 3.094669423\eta^2 + 0.007353959050\eta^7 \\ & - 0.008556567437\eta^6 - 0.07553413596\eta^5 \\ & + 0.00002328756731\eta^{10} + 0.00002738172826\eta^9 \\ & - 0.001371392391\eta^8, \end{aligned}$$

$$\begin{aligned} \theta(\eta) = {} & -14.10995285\eta + 14.110119089 \\ & - 28.11693674\eta^4 + 54.14756600\eta^3 \\ & - 29.48451471\eta^2 - 1.793625374\eta^7 \end{aligned}$$

$$+7.668438948\eta^6 - 2.197322558\eta^5$$

$$-0.02934726421\eta^{10} + 0.2414678217\eta^9$$

$$-0.4359641613\eta^8.$$

4. Results and discussion

The current research demonstrates the behavior of a steady Darcy-Forchheimer flow of (Al_2O_3-Cu/H_2O) through a stretching/shrinking rotating disk under multiple conditions, velocity slip, thermal radiation, and a convective boundary condition. The R-K technique was used to get the solution to the modified nonlinear coupled equations. Table 1 shows the clear-cut outputs of the base fluid and nanoparticles. Table 2 indicates a good agreement between the numerical results compared with the HPM in Maple. Figure 2 compares the HPM and the numerical method (R-K method) for velocity. It reveals the high accuracy of the HPM compared to the Numerical Method (NM). The homotopy perturbation approach and the numerical method (R-K method) for temperature are compared in Figure 3. The HPM is more accurate than the numerical approach. With $K = 0.12, Fr = 0.18, M = 0.5, Rd = 2.0, \eta = 0.2, \gamma = 0.1.\delta = 0.3, \Gamma = 0.1, Br = 5, D = 0.5, Ec = 0.1, Re = 0.1, Q = 0.15, Pr = 6.20, Y = 0.1, E_1 = 0.7, Bi = 1$ Figure 4 shows the impact of magnetic parameters on the velocity profile. In the case of stretching and shrinking, the velocity decreases as the magnetic parameter rises. This is because an increase in M indicates an increase in Lorentz force, which reduces the magnitude of the velocity. In both stretching and shrinking scenarios, higher values of the inertia coefficient Fr increase the velocity field, as shown in Figure 5. The effect of the electric field parameter E_1 on the velocity profile is seen in Figure 6. For increasing values of the electric field parameter, it is seen that the fluid velocity and its corresponding boundary layer thickness increase. Figure 7 shows the effect of magnetic parameter M on the velocity profile. In the case of stretching and shrinking, the velocity decreases as the magnetic parameter increases. This is because an increase in M indicates an increase in Lorentz force, which reduces the magnitude of the velocity. In both stretching and shrinking scenarios, with higher values of the inertia coefficient Fr, the velocity profile decreases, as shown in Figure 8. The influence of the electric field parameter E_1 on the velocity profile is seen in

Table 2. Comparison results of E_1 with NM and HPM for $\sqrt{2}A_1\sqrt{[F''(0)]^2 + [G'(0)]^2}$.

E_1	$\sqrt{2}A_1\sqrt{[F''(0)]^2 + [G'(0)]^2}$	
	NM	**HPM**
0.1	2.504658	2.509692
0.2	2.500882	2.506297
0.3	2.497269	2.503024
0.4	2.493818	2.499873
0.5	2.490532	2.496844

Table 1. Thermophysical properties of water (H_2O), copper (Cu), and aluminum oxide (Al_2O_3) [41].

Parameters	ρ **(kg/m^3)**	C_p **(J/kgK)**	k **(W/mK)**	$\sigma(\Omega m)^{-1}$
Water (H_2O)	997.1	4180	0.613	0.05
Copper (Cu)	8933	385	401	59.6×10^6
Aluminium oxide (Al_2O_3)	3970	765	40	35×10^6

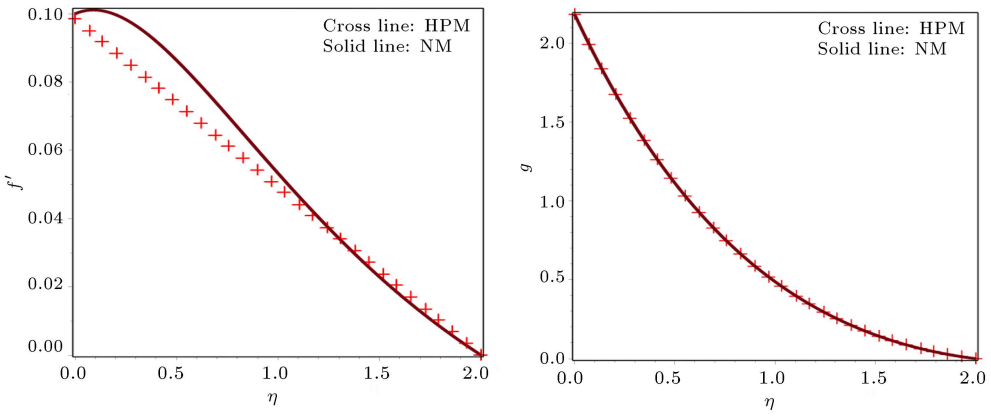

Figure 2. Comparison between HPM and NM for velocity profiles.

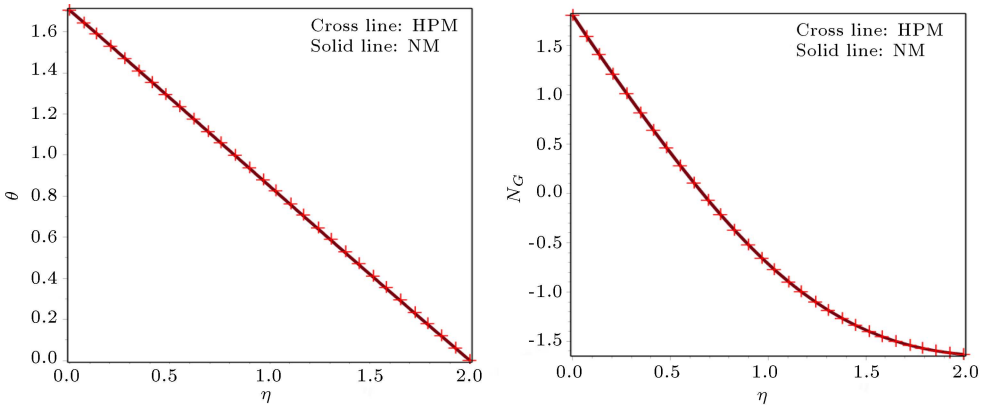

Figure 3. Comparison between HPM and NM for temperature and entropy generation profiles.

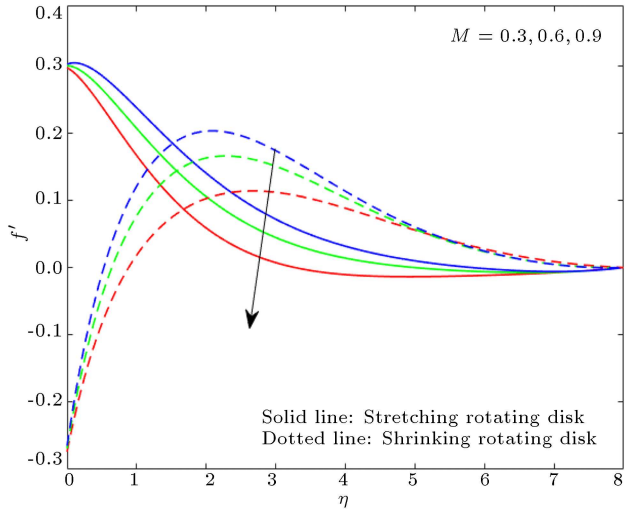

Figure 4. Variation due to M on $f'(\eta)$.

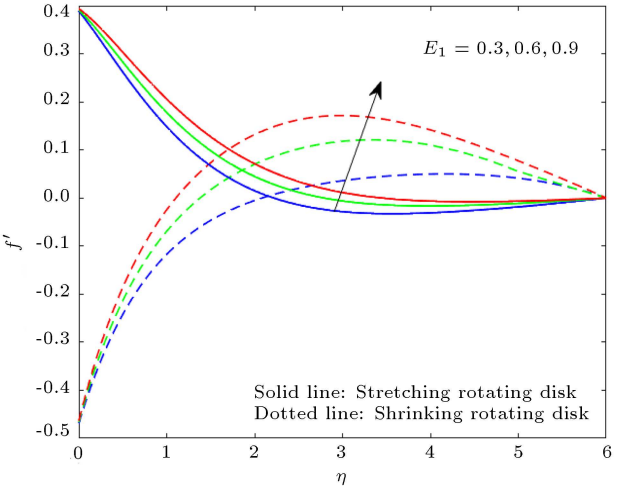

Figure 6. Variation due to E_1 on $f'(\eta)$.

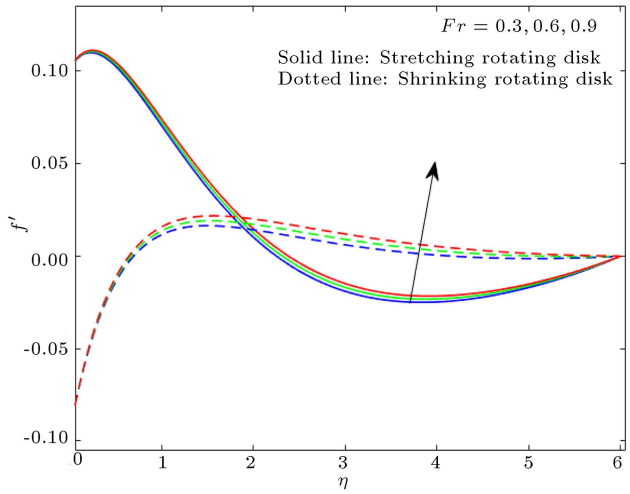

Figure 5. Variation due to Fr on $f'(\eta)$.

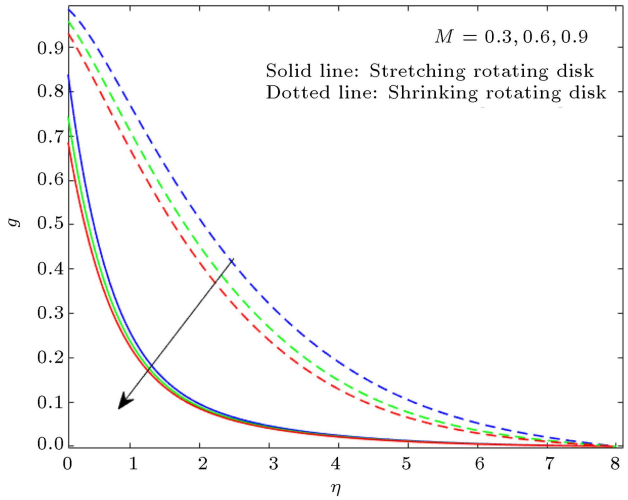

Figure 7. Variation due to M on $g(\eta)$.

Figure 9. The velocity profile enhances the higher values of the electric field. The larger values of the magnetic parameter M enhance the temperature profile, as shown in Figure 10. This is because a transversal magnetic field applied to an electrically conducting fluid causes the Lorentz force, which is a resistive form of force. This force has the effect of slowing the velocity of the fluid, thereby raising the temperature of the fluid. The effect of the electric field parameter on the temperature profile is seen in Figure

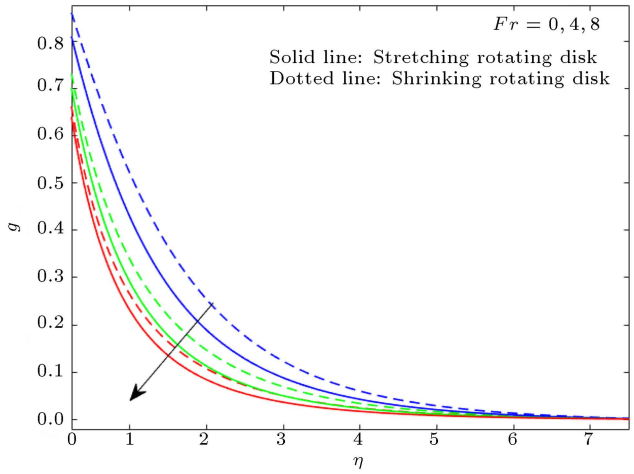

Figure 8. Variation due to Fr on $g(\eta)$.

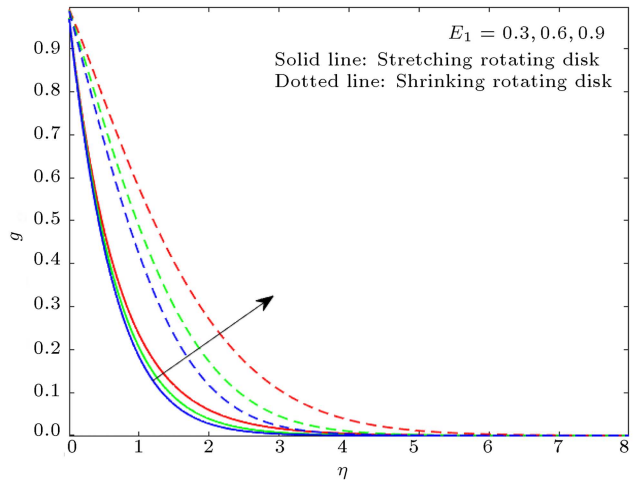

Figure 9. Variation due to E_1 on $g(\eta)$.

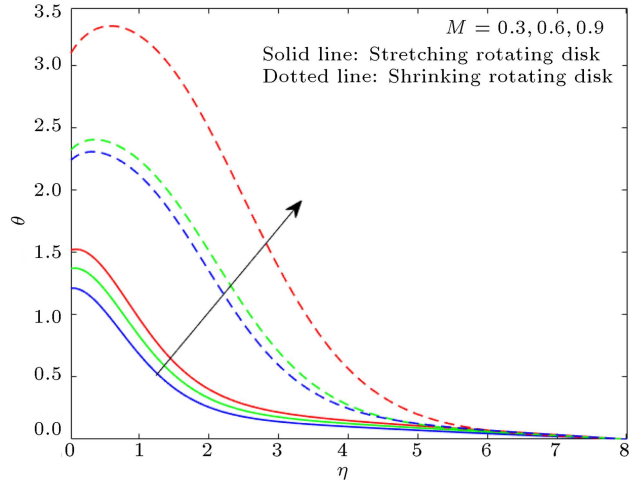

Figure 10. Variation due to M on $\theta(\eta)$.

11. For growing values of the electric field parameter, it is seen that the fluid temperature and corresponding thermal layer thickness increase. Figure 12 shows the influence of the heat generation parameter Q on

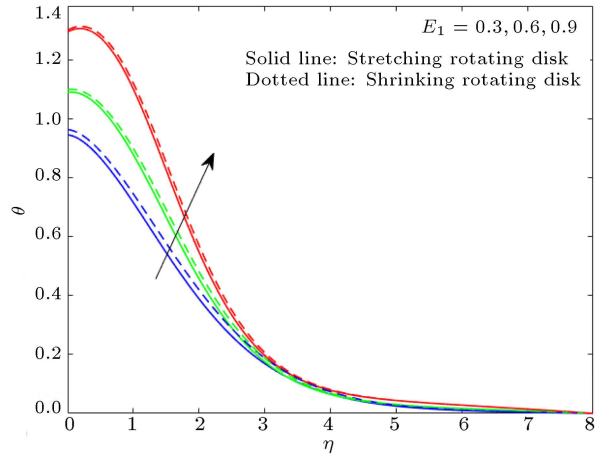

Figure 11. Variation due to E_1 on $\theta(\eta)$.

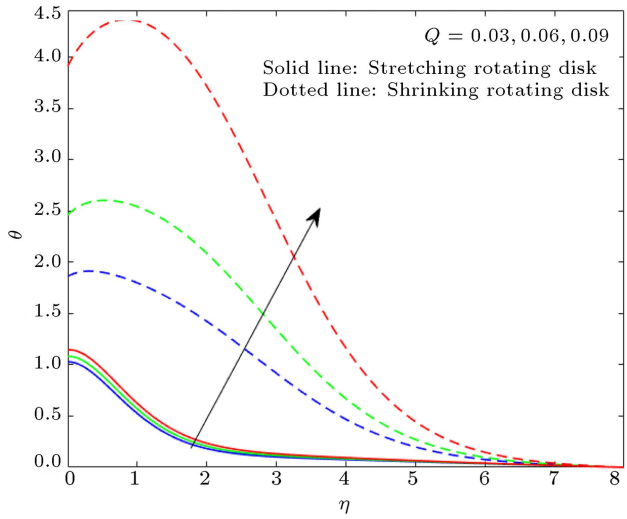

Figure 12. Variation due to Q on $\theta(\eta)$.

θ. Increasing the heat generation parameter increases the temperature profile in both cases of stretching and shrinking. Physically, the intrinsic energy of liquid particles grows by higher values of Q, and hence, temperature increases. Physically, increasing the radiation parameter Rd encourages more heat to enter into the liquid, which increases the thickness of the thermal boundary layer. As a result, in the high-emphasis flow area, radiation plays an important role in increasing the heat transfer rate from the disk surface, as seen in Figure 13. Figure 14 shows the impact of the wall slip parameter over the entropy generation profile when increasing the values of Γ. As a result, the entropy generation rate profile decreases. The effect of the Brinkman number on the entropy profile is seen in Figure 15. When increasing the values of the Brinkman number, the total entropy profile increases. Physically, the Brinkman number that rotates Br is the ratio of direct heat conduction from the disk surface to viscous heat produced by boundary layer shear. As Br increases, more heat is absorbed by the fluid,

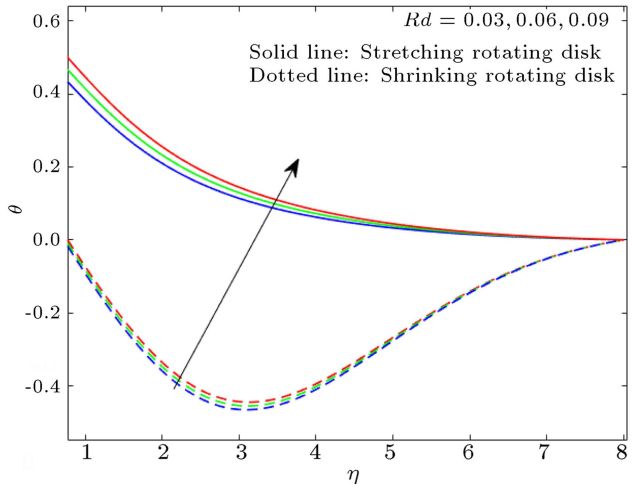

Figure 13. Variation due to Rd on $\theta(\eta)$.

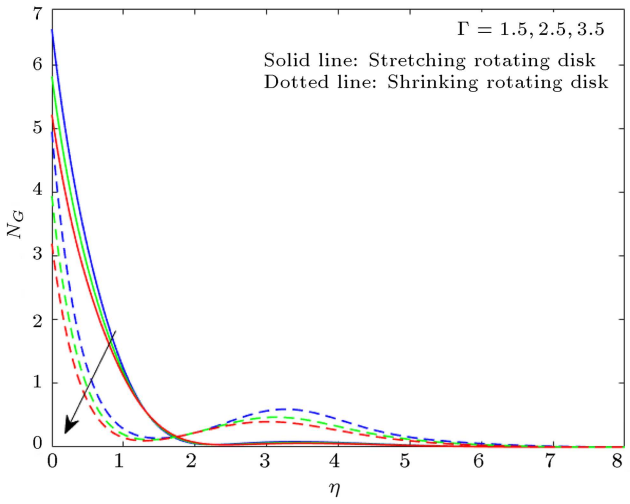

Figure 14. Variation due to Γ on N_G.

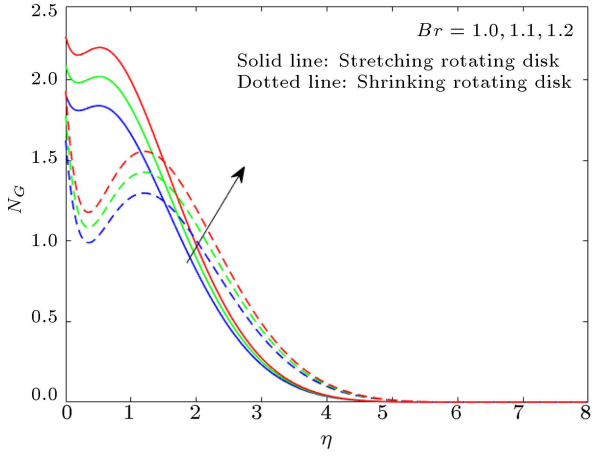

Figure 15. Variation due to Br on N_G.

significantly enhancing the gradient and growing the entropy generation profile. The variation in the entropy generation profile for different values of the ratio parameter is shown in Figure 16. It is observed that the

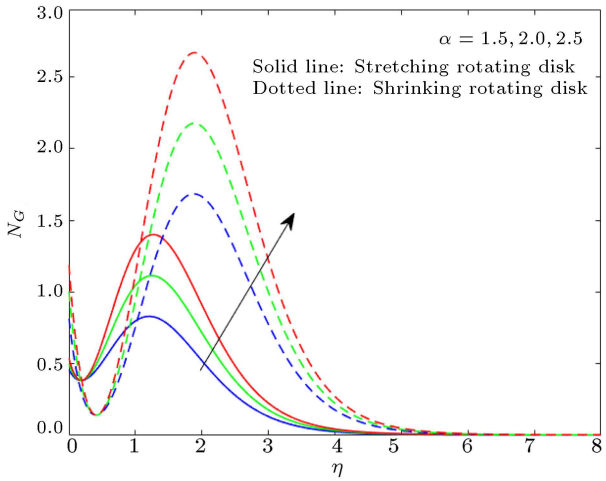

Figure 16. Variation due to α on N_G.

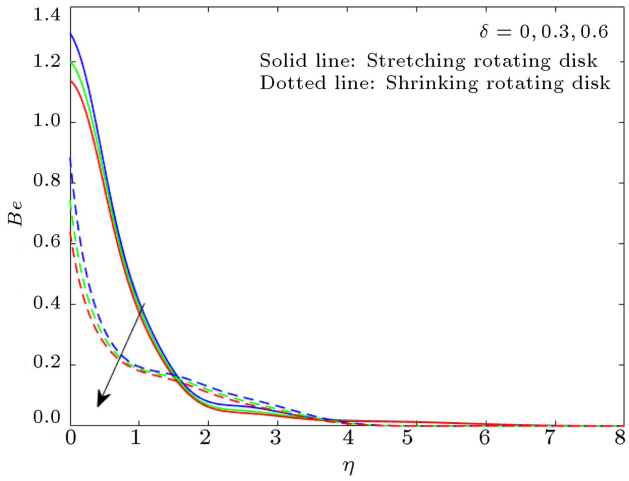

Figure 17. Variation due to δ on Be.

entropy generation profile increases with an increase in the ratio parameter. Figure 17 displays the influence that δ produces on the Bejan number profile when the higher values of δ are increased. Because of this, the Bejan number profile has decreased. In Figure 18, it is analyzed that the Bejan number profile improves for intensifying values of the Brinkman number.

Several factors on the skin friction coefficient were explored in Figure 19. Figure 19 shows the effect of the electric field and magnetic field on the skin friction coefficient. It shows that the skin friction coefficient grows in both cases of the greater values of electric field and magnetic field. Figure 20 displays the effect of the magnetic and electric fields on the Nusselt number. It demonstrates that the Nusselt number profile is increasing in both cases of the greater magnetic and electric field values.

5. Conclusions

In the present investigation, we have explored the entropy generation on electromagnetohydrody-

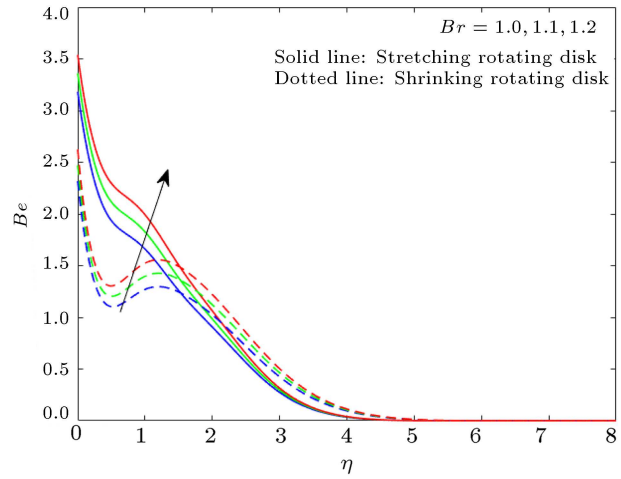

Figure 18. Variation due to Br on Be.

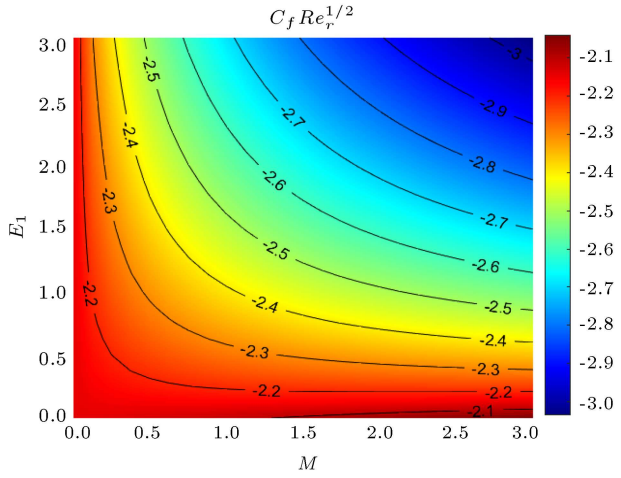

Figure 19. Impact of E_1 and M on $C_f(Re_r)^{1/2}$.

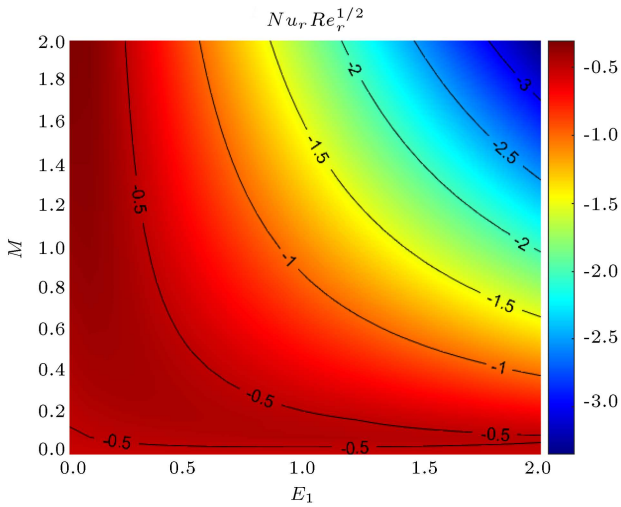

Figure 20. Impact of M and E_1 on $Nu_r(Re_r)^{-1/2}$.

namic (EMHD) copper-aluminum oxide/water hybrid nanofluid flow over a rotating disk. Self-similarity variables are used to transform non-dimensional partial differential equations. The effects of active parameters on velocities, temperature, entropy production, Bejan number, skin friction coefficient, and Nusselt number are graphically shown. This model may be useful for many modern industries that use them as heat exchangers and lubricants. The most important findings of this recent study are stated below:

- The velocity profile is enhanced by boosting the inertia coefficient parameter values;
- Electric field parameter leads to temperature profile enhancement;
- Temperature of fluid flow increased with the higher values of the thermal radiation (Rd) parameter;
- For the higher values of the Brinkman number and temperature ratio parameter, the entropy generation profile increases over a rotating disk;
- The Bejan number profile is enhanced in the case of higher values of the Brinkman number;
- The skin-friction coefficient and Nusselt number increase with the magnetic field parameter M increase;
- From an industrial point of view, the water/copper-alumina exhibits outstanding flow and thermal features.

Nomenclature

Parameter

(u, v, w)	Velocity components
(r, ϕ, z)	Directions (m/s)
k	Thermal conductivity ($W/m^{-1}/K^{-1}$)
ϕ_1, ϕ_2	Nanoparticles volume fraction
c_p	Heat capacity ($J/kg^{-1}/K^{-1}$)
T_w	Surface temperature (K)
T_f	Temperature of heated fluid (K)
T	Temperature of the fluid (K)
L	Wall slip coefficient
P	Pressure (Pa)
h_f	Heat transfer coefficient ($W/m^2/K$)
T_∞	Ambient fluid temperature (K)
E	Strength of electric field (N/C)
ϕ	Solid volume fraction
k^*	Mean absorption coefficient
K	Porosity parameter
Br	Rotational Brinkman number
Ec	Eckert number
γ	Stretching ratio parameter
Q	Heat absorption/generation coefficient

Γ	Wall slip parameter
Re	Rotational Reynolds number
Fr	Inertia coefficient
F^*	Non-uniform inertia coefficient
C_d	Drag coefficient
ΔT	Temperature difference
D	Dimensionless radial coordinate
Bi	Biot number
E_1	Electric field parameter
M	Magnetic interaction parameter
N_G	Dimensionless entropy generation rate
Rd	Radiation parameter
Ω	Curvature parameter

Greek letters

α	Temperature ratio parameter
μ	Dynamic viscosity ($kg/m^{-1}/s^{-1}$)
υ	Kinematic viscosity (m^2/s^{-1})
σ	Electric conductivity (s/m^{-1})
β	Thermal expansion (K^{-1})
ρ	Density (kg/m^{-3})
α_f	Thermal diffusivity of the base fluid (m^2/s)
σ^*	Stefan Boltzmann constant
τ_r	Radial wall stress (Pa)
τ_φ	Circumferential shear stress (Pa)

Subscripts

f	Base fluid
nf	Nanofluid
hnf	Hybrid nanofluid
s_1	First solid nanoparticle
s_2	Second solid nanoparticle

Superscript

$'$	Differentiation with respect to η

References

1. Shevchuk, I.V. "Convective heat and mass transfer in rotating disk systems", *Lect. Notes Appl. Comput. Mech.*, **45 LNACM**, pp. 1–9 (2009).
2. Choi, S. and Eastman, J. "Enhancing thermal conductivity of fluids with nanoparticles", No. ANL/MSD/CP-84938; CONF-951135-29 (1995).
3. Salahuddin, T., Awais, M., Khan, M., et al. "Analysis of transport phenomenon in cross fluid using cattaneo-christov theory for heat and mass fluxes with variable viscosity", *Int. Commun. Heat Mass Transf.*, **129**(October), p. 105664 (2021).
4. Rana, P. and Gupta, G. "Heat transfer optimization of Marangoni convective flow of nanofluid over an infinite disk with Stefan blowing and slip effects using Taguchi method", *Int. Commun. Heat Mass Transf.*, **130**, p. 105822 (2022).
5. Ayub, A., Sabir, Z., Shah, S., et al. "Effects of homogeneous-heterogeneous and Lorentz forces on 3-D radiative magnetized cross nanofluid using two rotating disks", *Int. Commun. Heat Mass Transf.*, **130**, p. 105778 (2022).
6. Reddy, S.R.R., Bala Anki Reddy, P., and Bhattacharyya, K. "Effect of nonlinear thermal radiation on 3D magneto slip flow of Eyring-Powell nanofluid flow over a slendering sheet with binary chemical reaction and Arrhenius activation energy", *Adv. Powder Technol.*, **30**(12), pp. 3203–3213 (2019).
7. Sadiq, M.A., Haider, F., Hayat, T., et al. "Partial slip in Darcy-Forchheimer carbon nanotubes flow by rotating disk", *Int. Commun. Heat Mass Transf.*, **116**, p. 104641 (2020).
8. Nayak, M.K., Mehmood, R., Makinde, O.D., et al. "Magnetohydrodynamic flow and heat transfer impact on ZnO-SAE50 nanolubricant flow over an inclined rotating disk", *J. Cent. South Univ.*, **26**(5), pp. 1146–1160 (2019).
9. Khan, U., Bilal, S., Zaib, A., et al. "Numerical simulation of a nonlinear coupled differential system describing a convective flow of Casson gold-blood nanofluid through a stretched rotating rigid disk in the presence of Lorentz forces and nonlinear thermal radiation", *Numer. Methods Partial Differ. Equ.*, **38**(3), pp. 308–328 (2022).
10. Waini, I., Ishak, A., and Pop, I. "Multiple solutions of the unsteady hybrid nanofluid flow over a rotating disk with stability analysis", *Eur. J. Mech. - B/Fluids*, **94**, pp. 121–127 (2022).
11. Sidik, N.A.C., Adamu, I.M., Jamil, M.M., et al. "Recent progress on hybrid nanofluids in heat transfer applications: A comprehensive review", *Elsevier*, **78**, pp. 68–79 (2016).
12. Reddy, P.B.A. "Biomedical aspects of entropy generation on electromagnetohydrodynamic blood flow of hybrid nanofluid with nonlinear thermal radiation and non-uniform heat source/sink", *Eur. Phys. J. Plus*, **135**(10), pp. 1–30 (2020).
13. Jakeer, S., Reddy, P.B.A., Mansour, M.A., et al. "Characteristics of moving hot block and non-Fourier heat flux model on sinusoidal wavy cavity filled with hybrid nanofluid", *Eur. Phys. J. Plus*, **137**(1), pp. 1–16 (2022).
14. Divya, A. and Reddy, P.B.A. "Electromagnetohydrodynamic unsteady flow with entropy generation and hall current of hybrid nanofluid over a rotating disk: An application in hyperthermia therapeutic aspects", *Institution of Mechanical Engineers, Part C: Journal of Mechanical Engineering Science*, **236**(13), pp. 7511–7528 (2022).

15. Ouyang, C., Akhtar, R., Raja, et al. "Numerical treatment with Lobatto IIIA technique for radiative flow of MHD hybrid nanofluid (Al_2O_3-Cu/H_2O) over a convectively heated stretchable rotating disk with velocity slip effects", *AIP Adv.*, **10**(5), p. 055122 (2020).

16. Hafeez, A., Khan, M., and Ahmed, J. "Flow of magnetized Oldroyd-B nanofluid over a rotating disk", *Appl. Nanosci.*, **10**(12), pp. 5135–5147 (2020).

17. Nayak, M.K., Mehmood, R., Makinde, O.D., et al. "Magnetohydrodynamic flow and heat transfer impact on ZnO-SAE50 nanolubricant flow over an inclined rotating disk", *J. Cent. South Univ.*, **26**(5), pp. 1146–1160 (2019).

18. Mustafa, M. "MHD nanofluid flow over a rotating disk with partial slip effects: Buongiorno model", *Int. J. Heat Mass Transf.*, **108**, pp. 1910–1916 (2017).

19. Iqbal, M.S., Mustafa, I., Riaz, I., et al. "Influence of carbon nanotubes on heat transfer in MHD nanofluid flow over a stretchable rotating disk: A numerical study", *Heat Transf.*, **50**(1), pp. 619–637 (2021).

20. Makinde, O.D., Mahanthesh, B., Gireesha, B.J., et al. "MHD nanofluid flow apst a rotating disk with thermal radiation in the presence of aluminum and titanium alloy nanoparticles", *Defect Diffus. Forum*, **384**, pp. 69–79 (2018).

21. Shah, Z., Dawar, A., Kumam, P., et al. "Impact of nonlinear thermal radiation on MHD nanofluid thin film flow over a horizontally rotating disk", *Appl. Sci. 2019*, **9**(8), p. 1533 (2019).

22. Sangapatnam, S., Ketineni, S., Chamkha, A.J., et al. "Numerical investigation of non-fourier flux theory with chemical action on maxwell radiating nanoliquid: A biomedical application", *Lect. Notes Mech. Eng.*, pp. 793–810 (2021).

23. Yuen, C. and Liu, Q. "A magnetic-field enriched surface-enhanced resonance Raman spectroscopy strategy towards the early diagnosis of malaria", *Biology and Medicine IX*, **8234**, pp. 98–103 (2012).

24. Bejan, A. "A study of entropy generation in fundamental convective heat transfer", *J. Heat Transfer*, **101**(4), pp. 718–725 (1979).

25. Bejan, A. "Second-law analysis in heat transfer and thermal design", *Adv. Heat Transf.*, **15**(C), pp. 1–58 (1982).

26. Suriya Uma Devi, S. and Mabood, F. "Entropy anatomization on marangoni Maxwell fluid over a rotating disk with nonlinear radiative flux and Arrhenius activation energy", *Int. Commun. Heat Mass Transf.*, **118**, p. 104857 (2020).

27. Khan, N., Riaz, I., Hashmi, M.S., et al. "Aspects of chemical entropy generation in flow of casson nanofluid between radiative stretching disks", *Entropy 2020*, **22**(5), p. 495 (2020).

28. Aziz, A. and Shams, M. "Entropy generation in MHD Maxwell nanofluid flow with variable thermal conductivity, thermal radiation, slip conditions, and heat source", *AIP Adv.*, **10**(1), p. 015038 (2020).

29. Jakeer, S. and Bala Anki Reddy, P. "Entropy generation on EMHD stagnation point flow of hybrid nanofluid over a stretching sheet: Homotopy perturbation solution", *Phys. Scr.*, **95**(12), p. 125203 (2020).

30. Jakeer, S., Bala Anki Reddy, P., Rashad, A.M., et al. "Impact of heated obstacle position on magneto-hybrid nanofluid flow in a lid-driven porous cavity with Cattaneo-Christov heat flux pattern", *Alexandria Eng. J.*, **60**(1), pp. 821–835 (2021).

31. Kasaeian, A., Azarian, R.D., Mahian, O., et al. "Nanofluid flow and heat transfer in porous media: A review of the latest developments", *Int. J. Heat Mass Transf.*, **107**, pp. 778–791 (2017).

32. Khan, M.I., Waqas, H., Khan, S.U., et al. "Slip flow of micropolar nanofluid over a porous rotating disk with motile microorganisms, nonlinear thermal radiation and activation energy", *Int. Commun. Heat Mass Transf.*, **122**, p. 105161 (2021).

33. Muskat, M. and Wyckoff, R., *The Flow of Homogeneous Fluids Through Porous Media*, McGraw-Hill Book Company (1946).

34. Khan, M.I., Alzahrani, F., Hobiny, A., et al. "Fully developed second order velocity slip darcy-forchheimer flow by a variable thicked surface of disk with entropy generation", *Int. Commun. Heat Mass Transf.*, **117**, p. 104778 (2020).

35. Shaw, S., Dogonchi, A.S., Nayak, M.K., et al. "Impact of entropy generation and nonlinear thermal radiation on darcy-forchheimer flow of MnFe2O4-casson/water nanofluid due to a rotating disk: Application to brain dynamics", *Arab. J. Sci. Eng.*, **45**(7), pp. 5471–5490 (2020).

36. Sadiq, M.A., Haider, F., Hayat, T., et al. "Partial slip in Darcy-Forchheimer carbon nanotubes flow by rotating disk", *Int. Commun. Heat Mass Transf.*, **116**, p. 104641 (2020).

37. Hayat, T., Qayyum, S., Imtiaz, M., et al. "Radiative flow due to stretchable rotating disk with variable thickness", *Results Phys.*, **7**, pp. 156–165 (2017).

38. Jakeer, S. and Reddy, P.B.A. "Entropy generation on the variable magnetic field and magnetohydrodynamic stagnation point flow of eyring-powell hybrid dusty nanofluid: Solar thermal application", *Proc. Inst. Mech. Eng. Part C J. Mech. Eng. Sci.*, p. 095440622110724 (2022).

39. Nayak, M.K., Patra, A., Shaw, S., et al. "Entropy optimized Darcy-Forchheimer slip flow of Fe_3O_4-CH_2OH_2 nanofluid past a stretching/shrinking rotating disk", *Heat Transf.*, **50**(3), pp. 2454–2487 (2021).

40. Ramasekhar, G. and Reddy, P.B.A. "Entropy generation on EMHD Darcy-Forchheimer flow of carreau

hybrid nano fluid over a permeable rotating disk with radiation and heat generation: Homotopy perturbation solution", *Institution of Mechanical Engineers, Part E: Journal of Process Mechanical Engineering*, **237**(4), pp. 1179–1191 (2023).

41. Rashad, A.M., Chamkha, A.J., Ismael, M., et al. "Magnetohydrodynamics natural convection in a triangular cavity filled with a Cu-Al_2O_3/water hybrid nanofluid with localized heating from below and internal heat generation", *J. Heat Transfer*, **140**(7), 072502 (2018).

Biographies

Gunisetty Ramasekhar was born in Andhra Pradesh, India, in 1997. He obtained an MSc degree in Applied Mathematics from the Yogi Vemana University, Kadapa, India, in 2020. He is a Researcher at Vellore Institute of Technology, Vellore, Tamilnadu. His research interests are mathematical modeling, fluid dynamics, properties of nanofluids, and their heat transfer characteristics.

Polu Bala Anki Reddy was born and raised in Andhra Pradesh, India. He obtained his MSc and PhD degrees in Mathematics from Sri Venkateswra University, Tirupathi, Andhra Pradesh. Presently, he is working as an Associate Professor in the Department of Mathematics, Vellore Institute of Technology, Vellore, Tamilnadu. Reddy research interest covers the areas of the application of flow separation, particularly in bio-fluid dynamics and analysis of boundary layer flows of Newtonian/non-Newtonian fluids, including the Entropy generation. Reddy research interest also covers the hybrid nanofluid flow with entropy generation. He published several papers in national and international journals. He attended several workshops/seminars/faculty development programs.